

Home Search Collections Journals About Contact us My IOPscience

Comparison of simulations on the NewMexico rotor operating in pitch fault conditions

This content has been downloaded from IOPscience. Please scroll down to see the full text.

2016 J. Phys.: Conf. Ser. 753 022049

(http://iopscience.iop.org/1742-6596/753/2/022049)

View the table of contents for this issue, or go to the journal homepage for more

Download details:

IP Address: 130.112.1.3

This content was downloaded on 20/10/2016 at 15:03

Please note that terms and conditions apply.

You may also be interested in:

Rotor thermal stress monitoring in steam turbines

Bouberle Antonín, Jakl Jan and Liška Jindich

Dynamics of the interaction between the rotor and the induction zone

Mahmood Mirzaei, Alexander R. Meyer Forsting and Niels Troldborg

Quantum to Classical Transition in a System of Two Coupled Kicked Rotors

Zhao Wen-Lei and Jie Quan-Lin

Stall-Induced Vibrations of the AVATAR Rotor Blade

M Stettner, M J Reijerkerk, A Lünenschloß et al.

CFD computations of the second round of MEXICO rotor measurements

Niels N. Sørensen, F. Zahle, K. Boorsma et al.

Simulations of wind turbine rotor with vortex generators

Niels Troldborg, Frederik Zahle and Niels N. Sørensen

Finding the ideal strategy: Full-scale fatigue testing of wind turbine rotor shafts

T Rauert, J Herrmann, P Dalhoff et al.

doi:10.1088/1742-6596/753/2/022049

Comparison of simulations on the NewMexico rotor operating in pitch fault conditions

L Oggiano¹, K Boorsma, G Schepers² and M Kloosterman³

- ¹ Institutt for Energiteknikk, Instituttveien 16a, 2007, Kjeller, Norway
- ² Energy research Centre of the Netherlands, Westerduinweg 3, 1755 LE, Petten, Netherlands

Luca.oggiano@ife.no

Abstract. The present paper aims to simulate and reproduce the experiments on a imbalanced rotor with one blade off pitched by 20degees carried out within the IEA task 29 Mexnext Phase III. Models of increasing complexity were used (Blade Element Method simulation (BEM) lifting line with free vortex wake (FVW) and URANS CFD) and the results were compared. The rotor has a diameter of 4.5m and three different load cases corresponding to a tip speed ratio of 5.24, 7.6 and11.2 were chosen from the test matrix performed during the experiments. The rotor speed was kept constant at 324.9RPM. BEM and FVW simulations were performed using the Aero Module tool developed by ECN that offers both an advanced BEM formulation and a FVW formulation named AWSM. The commercial solver STARCCM+ was for the CFD simulations and an Unsteady RANS approach with the k- ω SST turbulence model was chosen. Loads recorded with strain gauges during the experiments and pressures on the equipped blades were compared with results from the numerical simulations. The comparison provided good agreement in the low tip speed ratio cases while differences were more noticeable for the highest tip speed ration load case.

1. Introduction

In order to increase the power production thus reducing the energy production costs, malfunctions and fault conditions need to be taken into consideration and carefully studied.

Wind turbine controllers or mechanical faults could possibly lead to under or over pitching of one or more rotor blades with consequent rotor imbalance and increase in fatigue loads on bearings and gearbox but also to drastic change in power production. Even if guidelines for design and certification are prescribed in the IEC-61400-1 standard [1] and it is well known that pitch fault conditions are quite likely to happen in operational conditions [2], limited data is currently available and it is somehow unknown how the performance of each blade is affected by a pitch misalignment. Recent experiments on a rotor operating in pitch fault conditions were carried out within the IEA task 29 phase III [3] as continuation of the previous phases I [4] and II [5] in the DNW wind tunnel. In the experiments, the rotor was operated with one of the tree blades having a pitch offset (its pitch angle reduced by 20° in comparison to the other blades). The rotational speed was kept to 324 rpm to keep the instability and a full sweep through the operational regime was performed, featuring the standard pitch angles for blade 1 and blade 3.

While the current status in wind turbine modelling is mostly based on blade element momentum theory, it is well known that these methods are not applicable in highly unsteady flow, stalled

³ DNV-GLEnergy Utrechtseweg 306, B50 6800 ET, Arnhem, Netherlands

Content from this work may be used under the terms of the Creative Commons Attribution 3.0 licence. Any further distribution of this work must maintain attribution to the author(s) and the title of the work, journal citation and DOI.

doi:10.1088/1742-6596/753/2/022049

conditions and under yawed conditions due to the nature of the theoretical formulation behind them, which is based on independence between blade elements and actuator disk assumption. More generally, complex turbine conditions like yawed inflow, pitch asymmetry, or heavily deflected rotor that result in non-uniform induction like blades violate the assumptions of BEM and its correction models limiting its range of applicability [6, 7].

More sophisticated and elegant approaches which imply fewer limitations and a larger range of applicability are currently available. The lifting-line theory models combined with a free vortex wake method allow to reproduce the complex flow phenomena on wind turbine rotors and, even if local corrections are needed, lifting-line free vortex wake method (FVW) proved to be more accurate in determining wind turbine loads than BEM codes even in individual pitch conditions. Some examples that have been coupled to wind turbine simulations are the AWSM code developed at the Energy Research Centre of the Netherlands—the GENUVP code developed at the National Technical University of Athens [8] the WinDS code developed at the university of Massachussets [9], and the prescribed vortex model implemented in some versions of AeroDyn [10].

An even more advanced approach is to model the full rotor and solve the Reynolds-averaged Navier-Stokes equation (RANS) of the flow around the model. The RANS equations are averaged version of the governing equations where turbulent stresses are modelled in order to provide different levels of closure for the equations. With this approach, statistically unsteady (or non-stationary) flows can be treated [11, 12] and the near wake can be accurately computed [13, 14].

The present work aims to reproduce and simulate three selected cases from the text matrix tested in the wind tunnel with models of increasing complexity BEM, Actuator line with vortex method (FVW) and URANS CFD. BEM and FVW simulations were carried out using the Aero Module tool from ECN[15]. For the CFD simulations, the commercial software STARCCM+ from Cd-Adapco was used [16]. And an Unsteady RANS approach with the Menter [17] formulation of the k- ω SST turbulence model was used in the simulations. The results from the experiments were compared with the experimental values.

2. Methods

2.1. Experimental setup

The NewMexico rotor is a three bladed rotor model of 4.5 m diameter equipped with a speed controller and pitch actuator. The rotor blades specifically designed for the MEXICO wind tunnel measurement campaign and they are instrumented with 148 fast Kulite® XCQ-95-062-5 to measure the pressure distribution along the airfoil sections at different span locations The pressure sensors are distributed on the three blades (see Figure 1). Blade 1 (25% and 35% span), blade 2 (60% span),blade 3 (82% and 92% span).



Figure 1. The NewMexico rotor in the DNW wind tunnel (left) and the CAD model of the of the rotorwith blade 2 off-pitched (right).

In normal operational conditions, all the sensors are fully functional. For the pitch misalignment runs, the pitch angle of blade 2 was reduced by 20° in comparison to the other blades. The rotational speed was limited to 324 rpm to minimize instabilities. In the pitch misalignment test, the pressures were then measured only from the sensors placed in the tip area on blade 3 (82% and 92% span). The

doi:10.1088/1742-6596/753/2/022049

blades have been instrumented with strain gauges at the root of all three blades to measure the flatwise and edgewise root bending moments. The strain gauges were applied at 5 cm in spanwise direction from the blade root.

2.2. Blade description

The blades of the NewMexico turbine are the same used in the previous Mexico campaign and described in [3-5, 18]. The blade consists of three different aerodynamic profiles (DU91-W2-250, RISØ-A1-21 and NACA 64-418). The DU91-W2-250 airfoil is applied from 20 to 45.6% span, the RISØ-A1-21 airfoil from 54.4% to 65.6% span and the NACA 64-418 airfoil outboard of 74.4% span. The design pitch angle is -2.3deg.

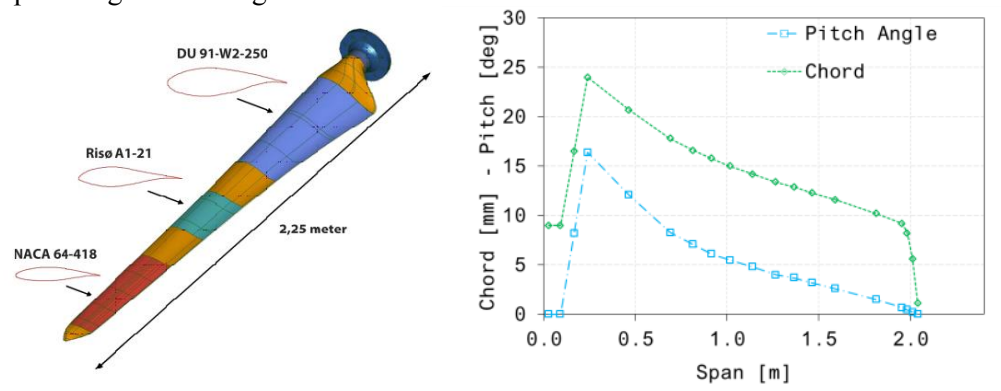


Figure 2. The Mexico Blade (left) and pitch/chord distribution along the blade span (right).

2.3. Load Cases

Table 1. Load cases.

Table 1. Load cases.						
	Load Cases	Wind Speed	Rotational speed	Pitch angle		Tip Speed Ratio λ
	_	(m/s)	(rpm)	Blade1,3 (deg)	Blade2 (deg)	-
	LC1	6.89	324.9	-2.3	-2.3	11.118
Normal	LC2	9.99	324.9	-2.3	-2.3	7.66
	LC3	14.52	324.9	-2.3	-2.3	5.274
	LC10FF	6.81	324.9	-2.3	-22.3	11.248
Fault	LC2OFF	9.97	324.9	-2.3	-22.3	7.667
	LC3OFF	14.56	324.9	-2.3	-22.3	5.259

Three load cases were chosen from the experimental test matrix for reduced rotational speed in order to represent three typical different operational conditions: a load case with low free stream velocity and high λ (LC1), a load case around design conditions (LC2) and a load case with low λ and high free stream velocity where the rotor operates in stalled conditions (LC3). Similarly, three load cases were chosen from the pitch misalignment test matrix so that the free stream velocity and thus the loads were comparable and they were named LC10FF, LC20FF and LC30FF. In these three load cases blade 1 and 3 were kept with the design pitch angle of -2.3 deg while blade 2 was pitched at -22.3 deg.

doi:10.1088/1742-6596/753/2/022049

2.4. Simulations

2.4.1. BEM and FVW (Aero Module)

The ECN Aero Module [15] was used for the lifting line calculations. It includes both BEM as well as a lifting line free vortex wake formulation, allowing the same external input (e.g. wind, tower, airfoil data) to be used for both models. The BEM formulation is based on PHATAS [19], including state of the art engineering extensions which have matured over decades of research in wind turbine rotor aerodynamics. The free vortex wake method is based on the AWSM code [20]. For the free vortex wake simulation with AWSM, the number of wake points was chosen to make sure that the wake length was developed over at least 3 rotor diameters downstream of the rotor plane. The wake convection was free for approximately 2 rotor diameters downstream. In addition to the BEM and AWSM free wake results, also AWSM simulations were ran using a prescribed wake formulation. A hybrid free-prescribed wake was adopted, drastically reducing the computational effort. Here only a small portion of the near wake was free, whilst the convection of the remainder was prescribed based on the calculated blade induction.

2.4.2. URANS CFD (Starccm+)

The multipurpose StarCCM+ code from CD-Adapco was used for the CFD simulations and, in the present work, an unsteady RANS (Reynolds Average Navier Stokes) approach was chosen to reproduce the experiments. A sliding mesh technique was used in the rotor plane for the URANS simulations to reproduce the rotor.

The full rotor consisting of three blades, hub and nacelle was modeled. The wind tunnel was not modeled. A trimmed meshing technique was used to discretize the rotor surface. The cell size on the surface was chosen so that the final grid consisted of a minimum number of 180 cells in the chordwise direction. A local surface grid refinement was applied at the leading edge. 15 cells in the boundary layer growing with a growing factor of 1.25 were used and the first cell placed so that a maximum wall y+ of 1 could be achieved on the blade, allowing thus the first cell to be placed in the viscous sublayer area of the boundary layer. A preliminary grid dependency study was carried out on a simpler configuration (one blade, 1/3 of the domain and steady state configuration) in order to ensure a grid independent solution in steady state conditions. A coarser mesh with only 5 cells layers of prismatic cells in the boundary region was generated on the nacelle and hub. The volume grid consisted of cubical cells with three cylindrical levels of grid refinement, progressive coarsening upstream and downstream was obtained by doubling the cell's characteristic length. refinement region, closer to the rotor plane, extends from -0.15m upstream to 0.4m downstream and it has a radius of 2.5m and a characteristic length of 0.02m, the second refinement region extends from -1m upstream to 1m downstream, it has a radius of 2.6m and it has a characteristic length of 0.4m and the third region extends from the inlet to 4m downstream, it has a radius of 4m and a characteristic length of 0.08m. A progressive coarsening was used in the rest of the domain (Figure 3).

The numerical wind tunnel has a square section of 30mx30m and a length of 80m. The rotor was placed at a distance of 15m from the inlet. The final mesh consisted of ca. 15.000.000 cells

Fully turbulent conditions were used in the simulations and the k- ω SST turbulence model introduced by Menter [17] was used throughout the whole simulation matrix. One degree per time step and 10 iterations per time step resulted to be sufficient in order to ensure convergence. A second order precision central difference numerical scheme was used to solve the Navier Stokes equations. A total number of 2 complete rotor revolutions were recorded and torque, thrust and pressure fields were averaged in time after the monitored values converged. Velocity inlet boundary conditions for the inlet, pressure outlet for the outlet and symmetry for the side walls were used in the simulation.

doi:10.1088/1742-6596/753/2/022049

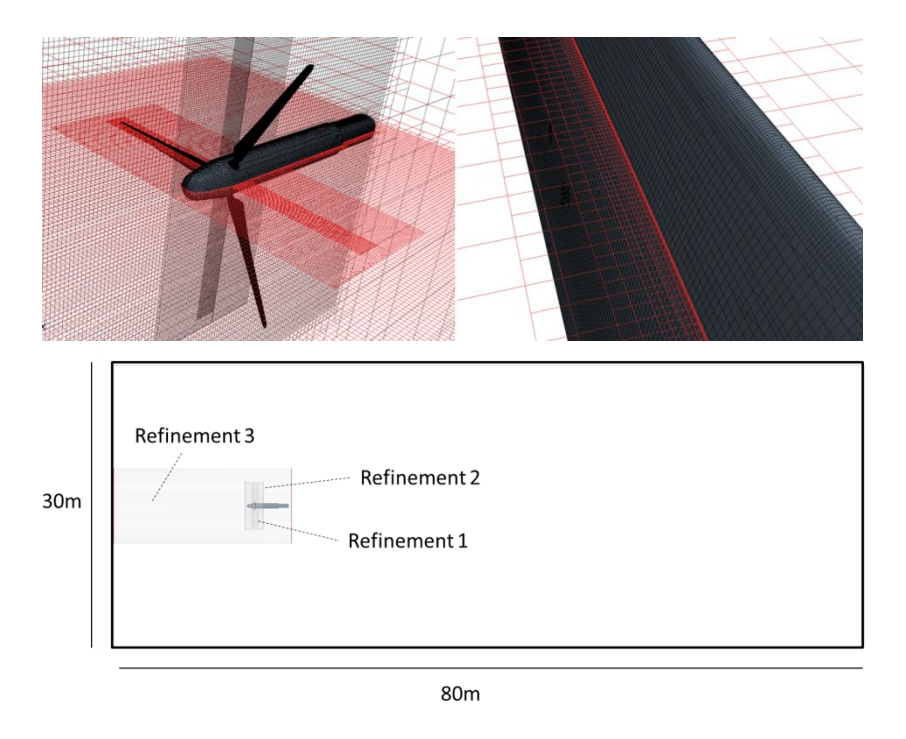


Figure 3. Mesh details and domain size

3. Results

In this section, the results obtained with URANS, FVW and BEM are presented and compared with the experimental data from the New Mexico campaign. Torque and axial force on each blade and on the total rotor are presented and pressure distribution on blade 3 from CFD simulations are compared with experimental values. Finally 3D effects are briefly discussed.

3.1. Axial Force and Torque on Full rotor and single blade

The results relative to all 6 load cases are presented in the histograms in Figure 4 and Figure 5. URANS simulations tend to overestimate the axial force Fax, particularly when the rotor is operating in stalled conditions and the k- ω SST turbulence model only partially manages to correctly reproduce the massively separated flow in the suction side of the blade. This behaviour is also clear when looking at the axial force on blade 2 for the off pitched load cases. With the turbine operating in design conditions, a general good agreement can be however found while larger differences and larger scattering between the models are noticeable in the fault conditions. All the models tend to overestimate the axial force.

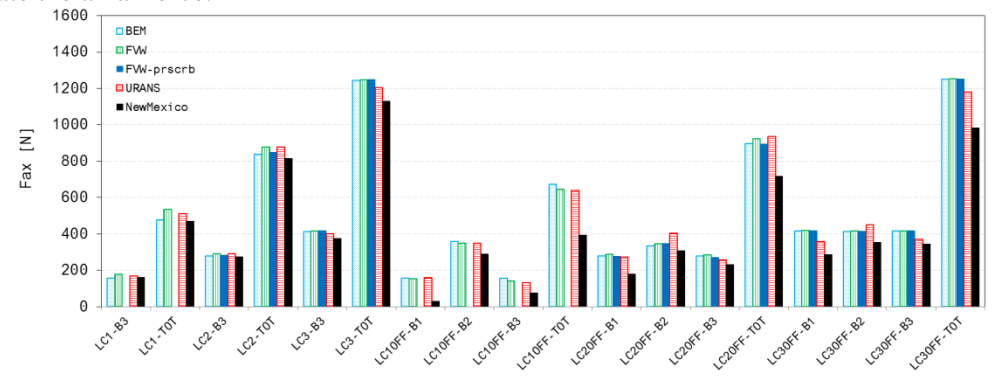


Figure 4. Comparison between thrust (Fax) from simulations and experimental values.

doi:10.1088/1742-6596/753/2/022049

Larger scattering between the models is noticeable when comparing the generated torque presented in Figure 5. All the models show an overall satisfactory comparison with the experimental data for normal operation conditions while larger scattering can be seen in the fault conditions especially in LC1OFF were the URANS simulations provide a better solution.

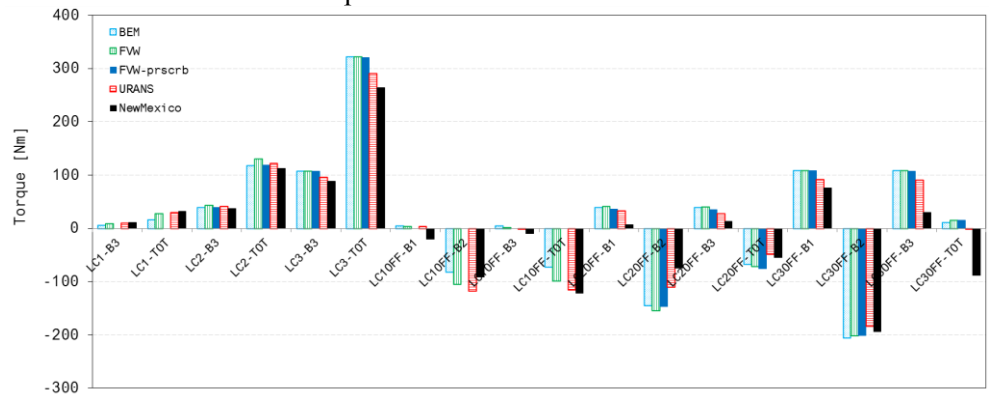


Figure 5. Comparison between generated torque from simulations and experimental values.

A similar trend can be seen in Figure 6 and Figure 7 where thrust coefficient (Cdax) and power coefficient (Cp) are plotted against the freestream velocity Minimal scattering between the models can be noticed for normal operational conditions while the differences are more pronounced in fault conditions. A comparison between normal operational and fault conditions shows that the overall measured performance of the rotor decreases in fault conditions with blade 2 operating in fully stalled conditions and generating lower axial loads and negative torque. None of the models was able to reproduce the decrease in total thrust visible in the experimental data.

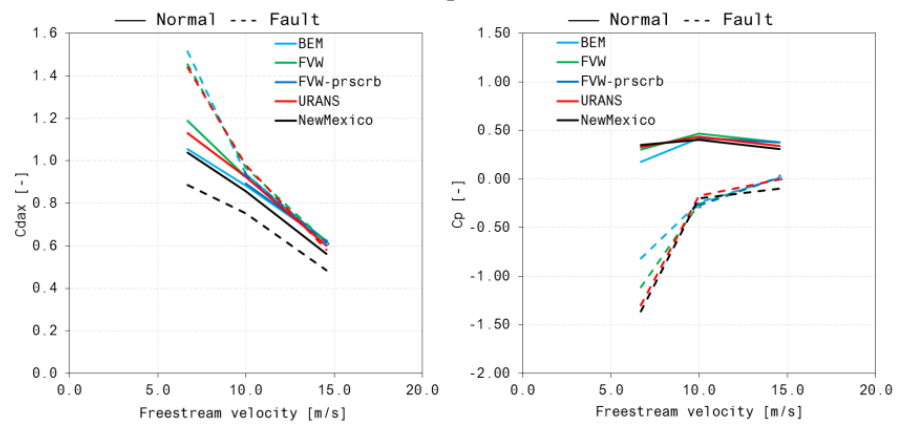


Figure 6. Thrust coefficient and power coefficient for Normal operational (Normal) and fault conditions (Fault) for the full rotor from simulations and experiments

However, all the models predict a larger axial force in fault conditions than in normal operational conditions. This is mostly due to the over prediction of the axial force on blade 2 in combination with a reduced force on the other two blades which is not properly accounted for. For the misaligned blade, the decrease in torque from operational to fault conditions is well predicted by all the models. In fault conditions, blade 3 operates in the turbulent wake created by the off-pitched blade 2 resulting in lower axial force and lower generated torque. The BEM model fails to predict the decrease in axial force for this blade showing similar levels to normal conditions. This is due to the fact that the blades are modelled independently in BEM, allowing no interference between them. For the FVW model this is different and a small decrease in axial force and torque is noticeable for the high tip speed ratio cases. Compared to the experiment the level decrease is very small due to the fact that lifting line methods do not explicitly model (drag dominated) separated flow areas, which is the major cause for the decrease. URANS simulations, due to a better resolution of the wake behind blade 2 are able to catch the trend

doi:10.1088/1742-6596/753/2/022049

but still overestimate the generated axial force and torque probably due to an underestimate of the velocity deficit in the tangential velocity.

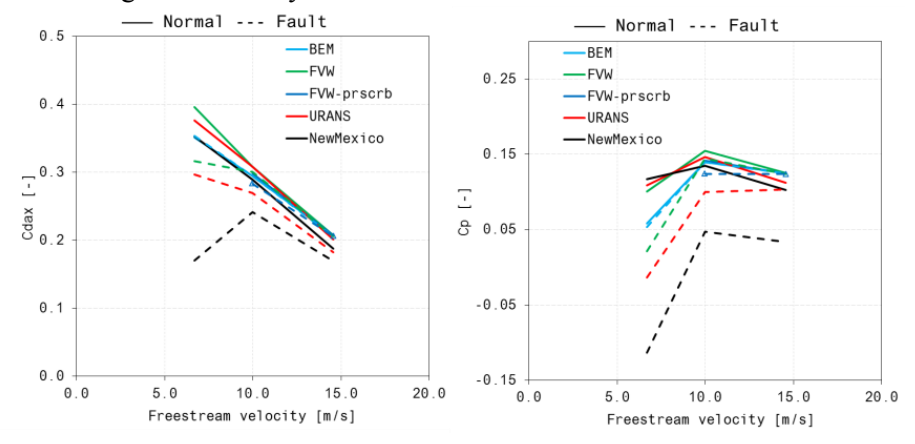


Figure 7. Axial force coefficient and power coefficient for Normal operational (Normal) and fault conditions (Fault) for blade 3 from simulations and experiments.

3.2. Pressure distributions on Blade3 from URANS simulations and Experiments

The pressure distribution plots along the blade are a useful tool in order to be able to better understand the loads acting on a wind turbine blade. The loads plotted on Figure 8 and Figure 9 **Figure 8** are relative to two sections of the blade 3 (82% and 92%) and refer to both normal operational conditions (LC1, LC2 and LC3) and fault conditions (LC1OFF, LC2OFF and LC3OFF). For lower freestream velocities or high tip speed ratios (LC1, LC1OFF) large differences between the normal operational and fault conditions can be seen. The large error bars visible in the experimental data for LC1 off at both 82% and 92% indicate that large fluctuations in pressure at the leading edge were measured. Since the fluctuations are limited to the leading edge area, large vibrations are probably excluded as a possible cause. A more likely explanation is the turbulent flow caused by the large separation behind blade 2. The iso-surface plots for the vorticity field in Figure 11 give a qualitative picture of the large vortices detaching from the tip area of blade 2 and hitting the tip of blade 1.

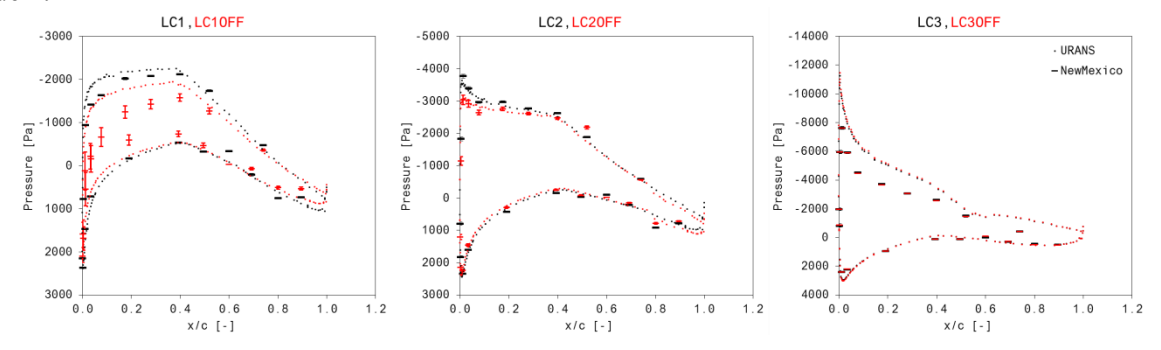


Figure 8. Pressure distribution plots at 82% span of blade 3 for normal operational (LC1,LC2 and LC3) and fault conditions (LC10FF,LC20FF,LC30FF) from experiments and URANS simulations.

The pressure plots from the URANS simulations show that the URANS approach is able to capture the trend but over predicts the loads. This behaviour is probably due to an incorrect estimate of the velocities in the separation area. With increasing wind speed (reduced tip speed ratio) the differences between the pressure plots for the operational conditions and fault conditions are reduced since the vortices generated by blade 2 are convected away from the rotor plane and blade 3 only partially sweeps in the turbulent wake generated by blade 2. In LC3 and LC3OFF, where the wind turbine is acting in stalled conditions, the pressure distributions plots for operational and fault conditions are overlapping each other both for the experiments and the URANS simulations. While the pressures on the pressure side of the blade are correctly computed, differences in this case are present in the suction

doi:10.1088/1742-6596/753/2/022049

side. This is a limitation of the RANS and URANS models that tend to over predict the negative pressure on the suction side of a wind turbine blade that operates in stalled conditions [5, 21].

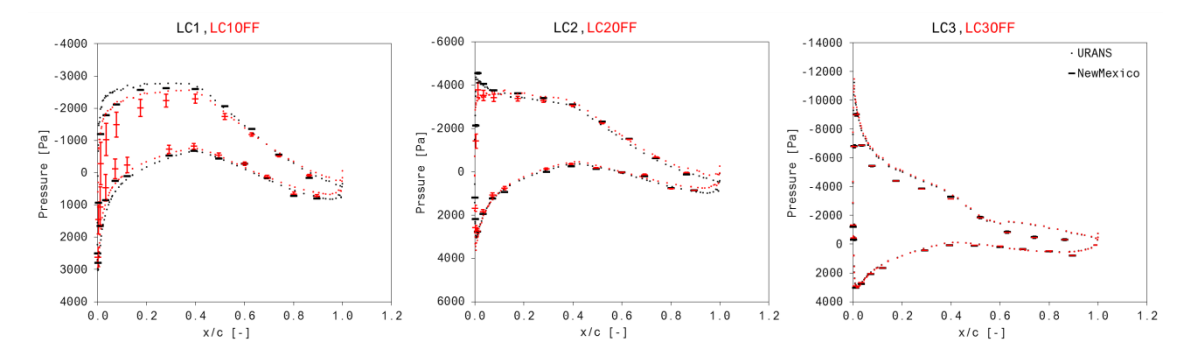


Figure 9. Pressure distribution plots at 92% span of blade 3 for normal operational (LC1,LC2 and LC3) and fault conditions (LC10FF,LC20FF,LC30FF) from experiments and URANS simulations.

From the contour plots on the blades in Figure 10 clear difference can be noticed when comparing LC1 with LC1OFF load case both in the pressure and suction side. On the pressure side, a higher pressure on the leading edge in experienced by the blade when operating in normal conditions and on the suction side a lower pressure is experienced by the blade along the span. Similar findings can be seen also comparing LC2 with LC2OFF and LC3 with LC3OFF. However, with increasing wind speeds the differences are less evident, as previously discussed.

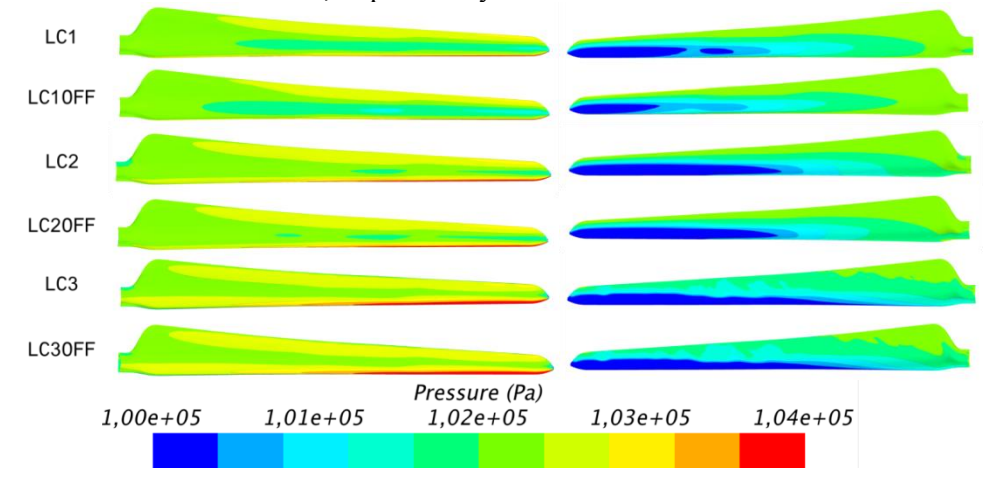


Figure 10. Contour pressure plots on the blades for pressure (left) and suction (right) side

A qualititative analysis of the vorticity (Figure 11) field for the three fault conditions show that for LC1OFF the long coherent vortical structures generated by blade 2 are kept and in the rotor plane and blade 3 sweeps through a highly turbulent area justifying the high standard deviation measured by the pressure sensors. With increasing velocity the vortical structures are covected in the streamwise direction behind the rotor and thus the incoming flow experienced by blade 2 and blade 3 is less influenced by the turbulence generated by the large structures detaching from blade 2. The stucture of the vortical structures is also affected and the vortices are broken into smaller structures.

doi:10.1088/1742-6596/753/2/022049

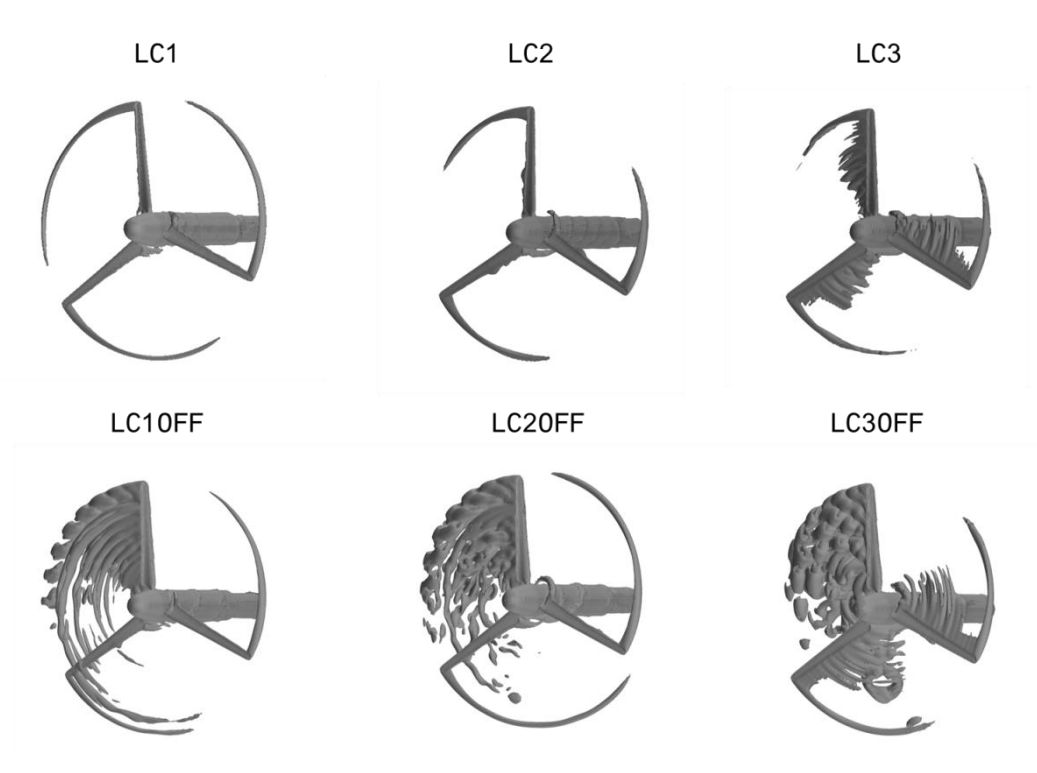


Figure 11. Iso vorticity fields for normal operational and fault conditions.

The same qualitative analysis is done for Figure 12 where the vorticity field on the rotor plane for the three fault load cases tested is represented showing that for LC10FF the vortex generated by blade 2 are confined to the rotor plane and blade 3 experiences an incoming flow affected by the vorticity generated by blade 2.

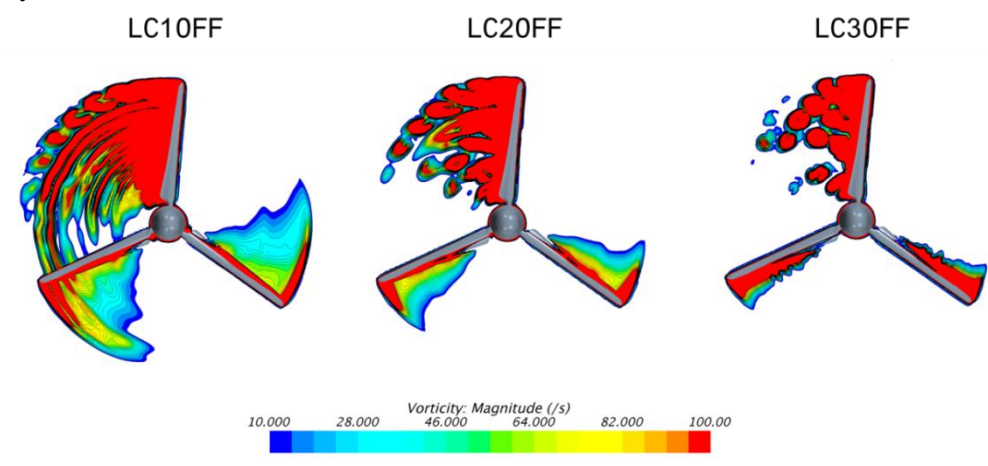


Figure 12. Vorticity field in the rotor plane

4. Conclusions

A comparison between models of increased complexity was featured in the present paper. All the models used are only partially able to reproduce the complex flow generated by the off pitched blade and the loads on the immediately following blade. All the models over predict the axial force generated both in normal and fault conditions but general trends are well predicted. BEM and to a lesser extent FVW experience difficulties in modeling the inflow conditions for the blade immediately following the off pitched blade while URANS simulations provide a better match with the

doi:10.1088/1742-6596/753/2/022049

experimental possibly due to a better prediction of the near wake and flow conditions in the rotor plane.

References

- [1] *IEC* 61400-1 Wind turbines Part 1 (design and requirements)
- [2] Tavner P J, J Xiang, and F Spinato 2007 Reliability analysis for wind turbines *Wind Energy* **10**(1) pp 1-18
- [3] Boorsma K and G Schepers 2014 New Mexico Experiment, Preliminary overview with initial validation (Technical Report ECN-E--14-048) ECN
- [4] Schepers J G et al. 2012 Final Report of IEA task 29, Mexnext (Phase 1): Analysis of Mexico wind tunnel measurements (Technical Report ECN-E–12-004) ECN
- [5] Schepers J G et al. 2014 Final report of IEA Wind Task 29: Mexnext (Phase 2) ECN
- [6] Snel H 1998 Review of the present status of rotor aerodynamics *Wind Energy* (1) pp 46–69
- [7] Leishman J G 2002 Challenges in Modelling the Unsteady Aerodynamics of Wind Turbines *Wind Energy* **5**(11) pp 85-132
- [8] Voutsinas S G 2006 Vortex Methods in Aeronautics: How to Make Things Work *Int. J. Comput. Fluid D.* **20** pp 3-18
- [9] Gaertner E M and L M A. 2015 Modeling Dynamic Stall for a Free Vortex Wake Model *Wind Eng.* **6** pp 675-691
- [10] Currin H D, F N Coton, and B Wood 2007 Dynamic prescribed vortex wake model for aerodyn 45th AIAA Aerospace Sciences Meeting and Exhibit
- [11] Herraez I et al. 2011 Simulation and validation of the MEXICO-Wind Turbine with OpenFOAM 6th OpenFOAM Workshop PennState University, USA 13-16 June
- [12] Gómez-Iradi S, R Steijl, and G N Barakos 2009 Development and Validation of a CFD Technique for the Aerodynamic Analysis of HAWT *J. Sol. Energy Eng.* **131**(3)
- [13] Schulz C et al. 2016 Investigations on the Wake Development of the MEXICO Rotor Considering Different Inflow Conditions *N. on Num. Fluid Mech. and Mult. Des.* **132** pp 871-882
- [14] Sørensen N N et al. 2012 Near wake Reynolds-averaged Navier–Stokes predictions of the wake behind the MEXICO rotor in axial and yawed flow conditions *Wind Energy* **17**(1) pp 75–86
- [15] Boorsma K, F Grasso, and J G Holierhoek 2012 Enhanced approach for simulation of rotor aerodynamic loads (Technical Report ECN-M–12-003) ECN
- [16] Cd-Adapco 2015 STARCCM+ Manual
- [17] Menter F R 1994 Two-equation eddy-viscosity turbulence models for engineering applications *AIAA J.* **32**(8) pp 1598–1605
- [18] Snel H, J G Schepers, and B Montgomerie 2007 The MEXICO project (Model Experiments in Controlled Conditions): The database and first results of data processing and interpretation *J. Phys. Conf. Ser.* **75**
- [19] Lindenburg C and J G Schepers 2000 Phatas-IV aeroelastic modelling, release (Technical Report ECN-CX-00-027 ECN) ECN
- [20] Van Garrel A 2003 Development of a wind turbine aerodynamics simulation module (Technical Report ECN-C-03-079) ECN
- [21] Li Y et al. 2012 Dynamic overset CFD simulations of wind turbine aerodynamics. *Renew. Energ.* **37** pp 285–298